Progress In Electromagnetics Research, Vol. 153, 123–131, 2015

Broadband Nanoantennas for Plasmon Enhanced Fluorescence and Raman Spectroscopies

Zhengdong Yong[1], Senlin Zhang[1], Yongjiang Dong[1], and Sailing He[1, 2, *]

Abstract—We propose a novel design of broadband plasmonic nanoantenna that is suitable for fluorescence and Raman enhancement. The structure consists of a gold nanoring and bowties at the center. We numerically investigate the near field and far field performance by employing the finite-difference time-domain method. High Purcell enhancement and large SERS are demonstrated in a record wide spectral bandwidth of 700 nm based on a single emitter-antenna configuration. Moreover, unlike a traditional antenna design, the proposed nanoantenna has low heat generation and high field enhancement at the gap simultaneously when operating off resonance.

1. INTRODUCTION

In the past decades, fluorescence and Raman spectroscopy techniques have emerged as powerful tools for analyzing labeled species, with a wide range of applications in chemistry [1], biomedicine [2, 3] and nano-optics [4]. While fluorescence results from the excitation of emitters by an incident field and the subsequent emission from an excited state to the ground state, which is determined by the competition between the radiative and non-radiative decay processes, Raman scattering is a purely inelastic scattering process between photons and molecules, mediated by vibrational or rotational modes of the molecules. Both can be used as complementary tools for examining the analyte, but are normally ineffective/weak due to the significant size mismatch between the wavelength of photons and the scale of emitters, which hampers the analysis of species at extremely low concentrations. Much effort has been made to improve the detection sensitivity, such as changing the scattering and absorption cross section via chemical approach [5] or a local electromagnetic field enhancement mechanism [6, 7].

Optical nanoantennas based on localized surface plasmon resonance [7, 8] are becoming more appealing since they can efficiently link far field radiation with the localized near field, allowing for high electromagnetic field enhancement, deep subwavelength confinement of light and tailoring of the local density of photonic states [4, 9, 10]. Fluorescence from emitters and Raman scattering of a molecule in the vicinity of plasmonic nanoantennas can be substantially enhanced, enabling the detection of species even down to single molecule level. Numerous types of nanoantenna configurations have demonstrated their ability to confine light at nanoscale and strongly enhance local fields, such as bowties [11, 12], nanorods [13], nanorings [14, 15] and clusters of nanoparticles [16]. However, most of these antennas are limited by the narrow band spectral response because of their dipolar nature, with a typical bandwidth at the order of 100 nm. Therefore, it is highly desirable and of great significance to design nanoantennas capable of broadband spectral responses for multispectral spectroscopy. Several topologies have been explored to achieve this, such as fractal geometry [17–19], multiple segments arrangement [20–22], log-periodic antennas [23–25] and nanocrescent antenna [26].

Received 24 September 2015, Accepted 3 November 2015, Scheduled 6 November 2015

* Corresponding author: Sailing He (sailing@kth.se).

[1] Centre for Optical and Electromagnetic Research, State Key Laboratory of Modern Optical Instrumentations, Zhejiang Provincial Key Laboratory for Sensing Technologies, Zhejiang University, Hangzhou 310058, China. [2] Department of Electromagnetic Engineering, School of Electrical Engineering, Royal Institute of Technology (KTH), S-100 44 Stockholm, Sweden.

However, they all have some limitations, for instance, the locations of hot spots in fractal antennas are wavelength dependent [17], the bandwidth of the multiple dipole antennas is constrained to the number of the resonant elements [20], and the photonic-plasmonic antennas require multi-periodic particle arrays [22]. Though trapezoidal log-periodic antennas analogous to their RF design [24, 27] and metacoxial antennas [28] are good candidates for multi-band operations, all these nanoantenna designs in the literature operate at resonance, with simultaneous large extinction cross section and large heat generation, which makes the structures fail under high power excitation. This aspect is commonly ignored with respect to the plasmon enhanced fluorescence and Raman spectroscopies. Here we propose a novel and compact antenna configuration that provides broadband near field enhancement in the same spatial position with low heat generation, and theoretically investigate the Purcell factor and Raman enhancement which has seldom been reported.

This paper is organized as follows. In Section 2, we show the theoretical background and the simulation methods of our broadband nanoantenna. In Section 3, we present the results and explain the working principle. First, we investigate the spectral response of the nanoantennas in Section 3.1. Then we study the fluorescence enhancement and SERS based on a single emitter-single antenna configuration in Section 3.2. In Section 3.3, we demonstrate that our antennas have low heat generation under illumination while maintaining high field enhancement. Finally, Section 4 provides the conclusions.

2. THEORY AND METHODS

Plasmonic nanoantennas show strong scattering and absorption under excitation in the visible and infrared regions due to their localized surface plasmonic resonances. The efficiency for each of these processes can be characterized by σ_{scat} and σ_{abs}, denoting the scattering and the absorption cross sections, respectively. The sum of these two cross sections is characterized by the extinction cross section $\sigma_{ext} = \sigma_{scat} + \sigma_{abs}$ [7]. The total absorbed power inside the nanostructures is transferred to the generated heat Q_{abs}, which is related to the field inside the structure via

$$Q_{abs} = \int_{np} Q_d dr, \quad Q_d = \frac{1}{2}\varepsilon_0 \omega \mathrm{Im}(\varepsilon_r)|E|^2 \tag{1}$$

where Q_d is the heat power density [29].

While heat generation is related to the field inside the nanostructure, fluorescence enhancement and SERS are highly dependent on the electric field outside the nanostructure. Consider an isolated emitter with radiative decay rate γ^0_{rad}, non-radiative decay rate γ^0_{nrad}, and define quantum efficiency $\eta_0 = \gamma^0_{rad}/(\gamma^0_{rad} + \gamma^0_{nrad})$. According to Fermi's Golden rule, the presence of plasmonic nanoantennas can strongly change the local electromagnetic environment, and thus modify the radiative decay rate and quantum efficiency of the emitter. We use the Purcell factor $F = \gamma_{rad}/\gamma^0_{rad}$ to represent the enhancement of the radiative decay rate and define the antenna efficiency $\eta_a = \gamma_{rad}/(\gamma_{rad} + \gamma_{nrad})$, where γ_{rad} and γ_{nrad} denote the modified radiative and nonradiative decay rates, respectively [13]. The modified quantum efficiency η then changes to

$$\eta = \frac{\eta_0}{(1-\eta_0)/F + \eta_0/\eta_a} \tag{2}$$

Since the fluorescence of the emitter is the product of the excitation and emission processes, under weak excitation (no saturation), the total fluorescence rate enhancement Γ_{em} can be expressed as

$$\Gamma_{em} = \Gamma_{exc} \cdot \eta/\eta_0 \tag{3}$$

where $\Gamma_{exc} = |E|^2/|E_0|^2$ represents the near field enhancement during the excitation process. We also use this defined electromagnetic enhancement factor $G_{(\omega)} = |E_{(\omega)}|/|E_0|$ to study the SERS. Unlike fluorescence, the total electromagnetic contribution to SERS can be expressed as $R = G^2_{(\omega_i)} G^2_{(\omega)}$, where ω_i is the excitation frequency and ω is related to the Stokes or anti-Stokes frequency. It becomes a usual E^4 dependence when the Raman scattering frequency is close to the excitation frequency [7].

Three-dimensional finite-difference time-domain calculations were performed using commercially available software package (Lumerical FDTD Solutions Inc.v8.6) to model the broadband nanoantenna [30]. The top view of the proposed broadband nanoantenna is shown in Fig. 1. It consists

of a gold nanoring and bowtie antenna at the center (BCR), both of which have been previously and thoroughly studied [11, 14]. Bowtie antennas were chosen because of their strong field localization, while the nanoring can exhibit remarkably uniform field enhancement in the ring interior. For gold bowtie antennas, the relevant parameters are the arm length L, gap size g_1, and opening angle θ. For the nanoring, the inner radius and the thickness of ring are R_i and T_r, respectively. They are separated by a small gap size g_2. Considering the fabrication limits and in order to avoid sharp edges, we model the bowtie tips as rounded with a radius of curvature of 10 nm. The initial geometrical parameters of the antennas are as follows: $L = 60$ nm, $\theta = 40°$, $g_1 = 10$ nm, $R_i = 75$ nm, $T_r = 135$ nm, $g_2 = 10$ nm, and the heights of the bowtie and ring is fixed to 40 nm. The optical constant of the gold is modeled by a Drude-Lorentz fitting (with 6 coefficients) to tabulated experimental data [31], and we assume the whole structure is embedded in water ($\varepsilon = 1.77$). A perfectly matched layer was employed in every face of the simulation box. To study the near field and far field performance of a single antenna, the solver-defined total-field scattered-field (TFSF) source polarized in the x-direction was normally incident to the nanoantenna ($-z$ direction), as shown in Fig. 1. Extinction cross section is calculated by summing the scattering and absorption cross sections. The total heat generation and heat power density can be obtained according to Equation (1), where we choose the incident power density as $1\,\text{mW}/\mu\text{m}^2$, a typical value found in literature [32]. To simulate the emission process modified by nanoantennas, a point dipole source oriented in the x direction acting as an isolated emitter is placed at the center of the gap region, which is represented by a red point in Fig. 1. The radiated emitted power P_{rad} and the total emitted power P_{tot} in the presence of the antenna were calculated by integrating the power flow over a closed surface surrounding the dipole source at respective distances of 1 μm and 2 nm. Then, the total and radiative decay rates enhancement can be obtained by normalizing the emitted power to the radiated emitted power P_0 of the same dipole source in the absence of the antenna: $\Gamma_{rad} = P_{rad}/P_0$ and $\Gamma_{tot} = P_{tot}/P_0$, here $\Gamma_{rad} = F$ and $\eta_a = \Gamma_{rad}/\Gamma_{tot}$ [4].

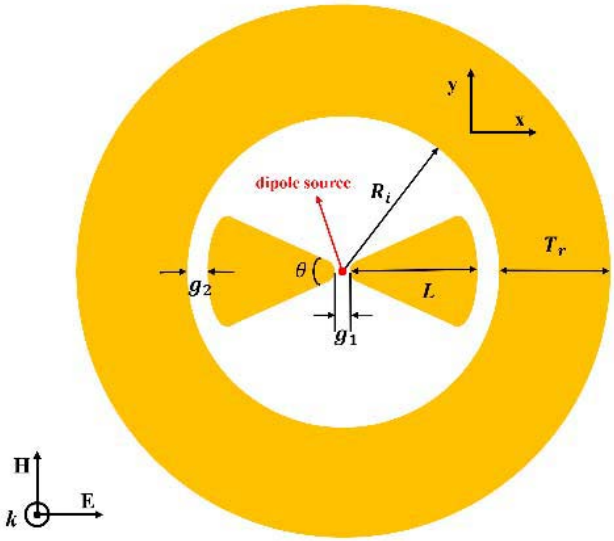

Figure 1. Top view of the plasmonic nanoantenna with broadband near field enhancement. It consists of a gold nanoring and a bowtie antenna at the center (BCR). The whole structure is immersed in water.

3. RESULTS AND DISCUSSIONS

3.1. Near Field Characteristics of Plasmonic Modes

The optical intensity enhancement with respect to the incident field at the center of the gap is plotted in Fig. 2(a), and a single bowtie antenna without ring and bowtie antenna designed for a wavelength of 850 nm are also compared. It shows that our antenna has two pronounced resonance peaks at

$\lambda_1 = 850\,\text{nm}$ and $\lambda_2 = 1300\,\text{nm}$, with a relatively large field enhancement in a broad spectral range, as defined by the full-width-half-maximum (FWHM) bandwidth about 700 nm while the FWHM of a single bowtie antenna is only 100 nm. The near field distributions 2 nm above the structure in the x-y plane at these two resonance wavelengths are illustrated in Fig. 2(b), and it is observed that the electric field is well confined around the gap at both wavelengths. With regard to the resonance at $\lambda_1 = 850\,\text{nm}$, the field pattern is only concentrated around the bowtie antenna, while at $\lambda_2 = 1300\,\text{nm}$, strong field is also observed around the outer ring. To further understand the characteristics of these two plasmonic modes, the charge distribution is also displayed in Fig. 2(b). The symmetric mode of the ring is well excited at

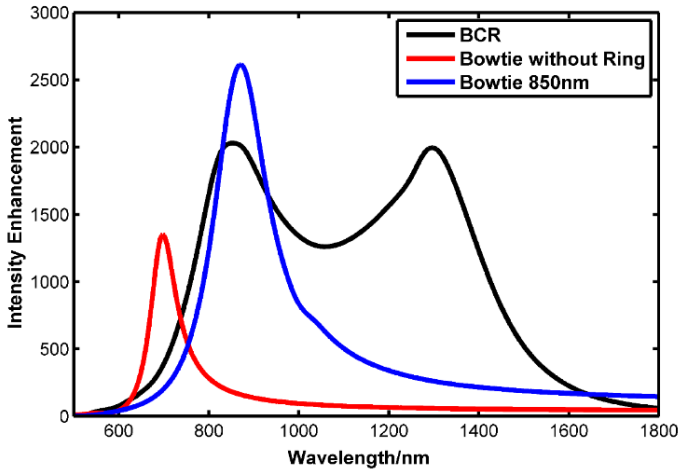

(a)

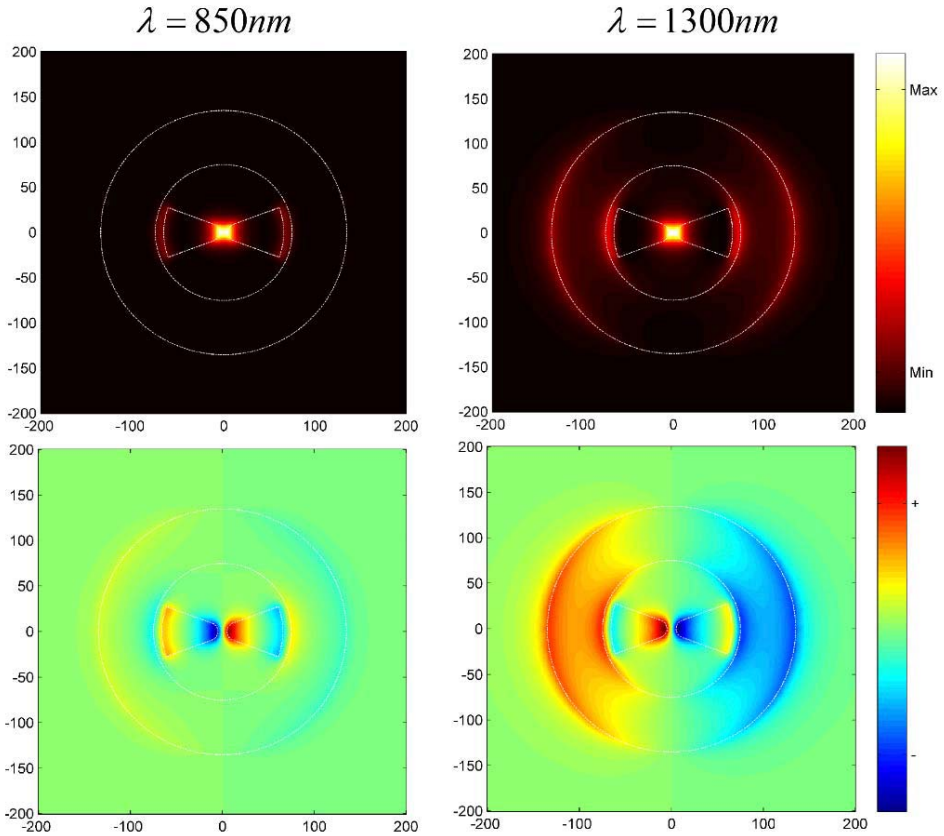

(b)

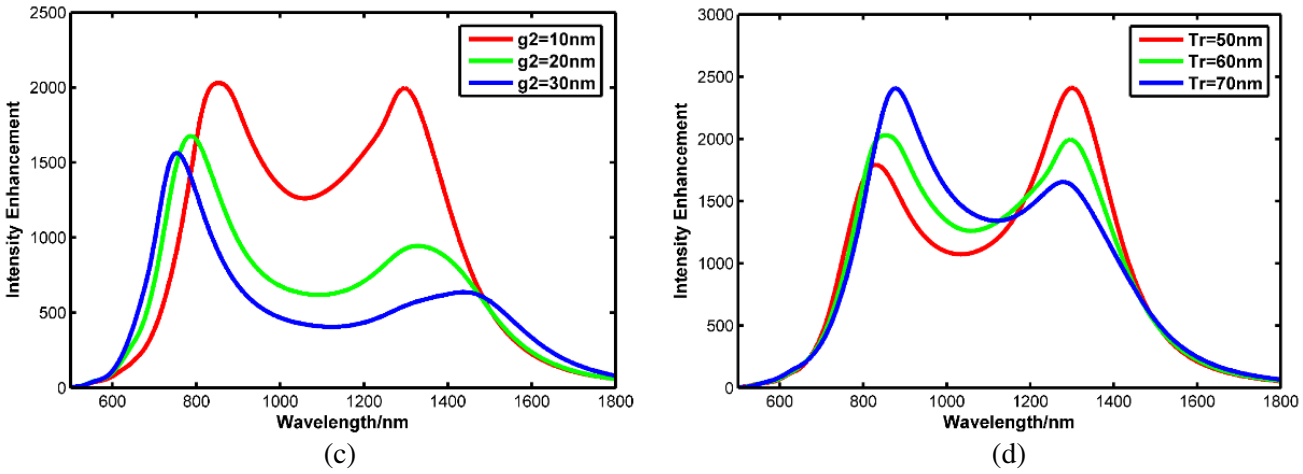

Figure 2. (a) Simulated near-field intensity enhancement spectra at the middle point of the gap of the BCR (black), bowtie without ring (red) and bowtie design for 850 nm (blue). (b) Normalized electric field (up row) and charge distributions (bottom row) for illumination at $\lambda = 850$ nm (left) and $\lambda = 1300$ nm (right). Intensity enhancement spectrum with different parametric studies. The red, green and blue curves correspond to (c) $g_2 = 10$ nm, 20 nm and 30 nm; and (d) $T_r = 50$ nm, 60 nm and 70 nm.

$\lambda_2 = 1300$ nm [14]. We may first infer that the first resonance is mainly ascribed to the bowtie antenna, while the nanoring contributes to the second long-wavelength resonance. Moreover, it is very interesting that when combined with the nanoring, a single narrowband bowtie antenna gives a broadband near field response, as shown in Fig. 2(a). Thus the nanoring plays a critical role in this broadband antenna. In the following, we will first change the separation distance between the bowtie and ring (g_2) and then change the geometrical parameters of the nanoring while keeping the other parameters the same. It is observed in Fig. 2(c) that when increasing g_2 from 10 nm to 30 nm, the second resonance sharply decreased and the first resonance is blue-shifted near to the resonant wavelength of a single bowtie, which shows the importance of the strong coupling between the ring and bowties. Fig. 2(d) shows that by increasing the thickness of the nanoring, the second resonance peak decreases with a blue-shift while the first is enhanced with a red-shift. This can be understood by considering the charge distributions that cause these two resonances in Fig. 2(b).

3.2. Broadband Purcell Enhancement and Raman Enhancement

The radiation dynamic of quantum emitters can be modified by the local density of the optical states, which was first studied by Purcell [33]. For a dipole source located at the center of the antenna and polarized along the x-axis, the Purcell factor F and antenna efficiency η_a are calculated as mentioned above and plotted in Fig. 3(a). For a dipole polarized with an angle θ to the x-axis, a factor of $\cos^2\theta$ is introduced according to partial local density of states [4]. It is observed that a Purcell enhancement over 1000 and antenna efficiency over 75% are achieved in a wide bandwidth of 600 nm. To our best knowledge, such broadband and high Purcell enhancement has not been achieved so far. For completeness, the modified quantum efficiency and the total fluorescence enhancement are also calculated according to Equations (2) and (3), and displayed in Fig. 3(b), where we assume a fluorescent molecule located at the center of the gap with intrinsic quantum efficiency $\eta_0 = 0.3$ and under weak excitation condition. Previous studies have demonstrated that low-quantum efficiency emitters have much higher fluorescence enhancement than high quantum efficiency emitters [34, 35]. Due to the large Purcell factor, the modified quantum efficiency is approximate to the antenna efficiency, and the intrinsic quantum efficiency is improved by the antenna. Thus, both the excitation rate and quantum efficiency enhancement contribute to the enhancement of the total fluorescence rate, and a thousand-fold fluorescence enhancement can be provided by the broadband nanoantenna.

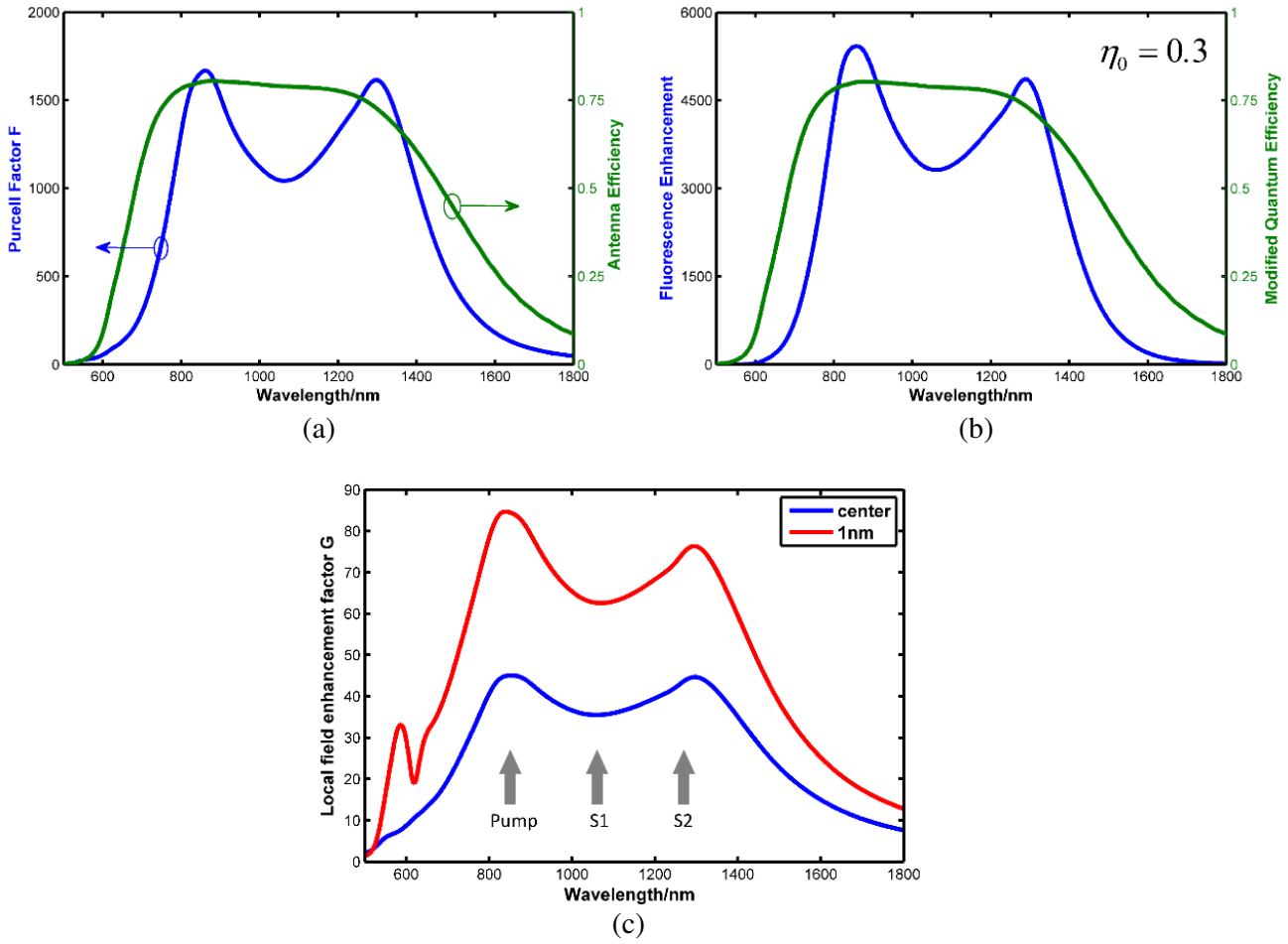

Figure 3. (a) Normalized Purcell factor F (blue) and antenna efficiency η_a (green) of the broadband antenna. A single electric dipole source was placed at the center of the gap. (b) Normalized fluorescence enhancement (blue) and modified quantum efficiency (green) of a single emitter with intrinsic quantum efficiency 0.3. (c) Local field enhancement factor G as the wavelength. The parameters of the structure are $L = 60\,\text{nm}$, $\theta = 40°$, $g_1 = 10\,\text{nm}$, $R_i = 75\,\text{nm}$, $T_r = 135\,\text{nm}$, and $g_2 = 10\,\text{nm}$.

To study the SERS enhancement, we calculate the local field enhancement factor G at the center of the gap and 1 nm close to the bowtie tip separately, shown in Fig. 3(c). A broadband and high G factor is observed near the antenna, though it is still lower than other reported values. Such an antenna design will fulfill SERS regardless of whether the Stokes line is close to the excitation wavelength or not, and different Raman signals from various molecules can be enhanced simultaneously, as the total electromagnetic contribution to SERS is $R = G^2_{(\omega_i)} G^2_{(\omega)}$. For example, when exciting at the pumping wavelength as shown in Fig. 3(c), the Stokes signal at S_1 and S_2 are both enhanced, this is much similar to the concept of double resonance Raman enhancement [36, 37], but more practicable.

3.3. Heat Generation

Due to the intrinsic high loss of the localized plasmons, plasmonic nanoantennas have large heat generation at resonance, which makes the structure fail under high power excitation. Fig. 4(a) shows the extinction cross section along with the near field enhancement at the center of gap of the proposed antenna. In the wavelength region between the two resonant peaks, the extinction cross section decreases due to its non-resonant characteristic while the near field enhancement still maintains a high value.

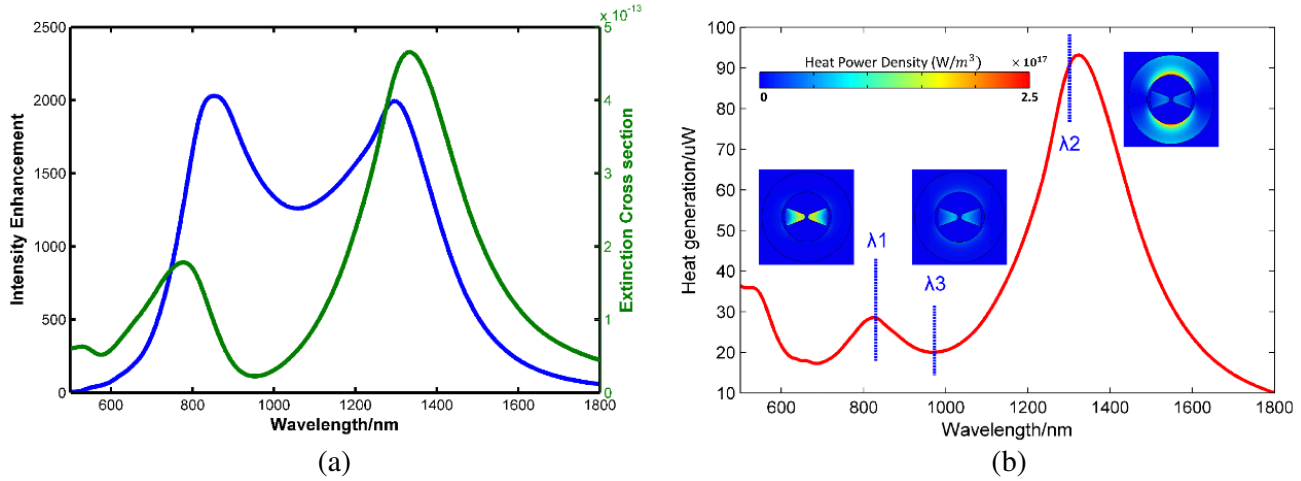

Figure 4. (a) Field intensity enhancement spectra (blue) and extinction cross section (green) of the structure. (b) Calculated spectra of the heat generation in antennas immersed in water. The three insets represent the heat power density at λ_1, λ_2 and λ_3.

Furthermore, heat generation under excitation power density $1\,\mathrm{mW}/\mu\mathrm{m}^2$ is calculated and shown in Fig. 4(b). We see two resonant peaks around $\lambda_1 = 850\,\mathrm{nm}$ and $\lambda_2 = 1300\,\mathrm{nm}$, with the second peak much larger than the first one. This is due to the additional magnetic dipole contribution and larger volume according to the charge distribution in Fig. 2(b). Here we mainly focus our attention on the dip region around $\lambda_3 = 1000\,\mathrm{nm}$, with the same reason as the dip in the extinction cross section in Fig. 4(a). The insets in Fig. 4(b) represent the heat power density at respective wavelengths. Consistent with the above near field characteristic, the heat power density is concentrated in the body of the bowtie antenna at $\lambda_1 = 850\,\mathrm{nm}$, while it is redistributed in the body of the ring at $\lambda_2 = 1300\,\mathrm{nm}$. The heat power density distribution at $\lambda_3 = 1000\,\mathrm{nm}$ is more uniform with a relatively low value. This off-resonance operation makes this broadband antenna more applicable than the traditional resonant antennas.

4. CONCLUSIONS

In summary, we have proposed and numerically demonstrated a novel plasmonic nanoantenna with broadband near field enhancement in the same spatial position. The strong electromagnetic field enhancement simultaneously enables high Purcell and Raman enhancements. Thousand-fold fluorescence enhancement and antenna efficiency over 75% in a wide bandwidth of 700 nm have been demonstrated based on single antenna-emitter configurations. Broadband SERS have also been achieved regardless of whether the Raman molecules have a long wavenumber, making it more practicable than the single resonant antennas. Furthermore, the total heat generation and heat power density have been investigated numerically. Compared with the usual resonant design, this non-resonant enhancement with lower heat effect shows significant improvement and opens up a new path for plasmon enhanced fluorescence and Raman spectroscopies. It is expected that this broadband nanoantenna holds great potential in other nonlinear applications such as harmonic generation [38] and nanolasers [39].

ACKNOWLEDGMENT

This work was partially supported by the National Natural Science Foundation of China (Nos. 91233208 and 61178062), the National High Technology Research and Development Program (863 Program) of China (No. 2012AA030402), the Program of Zhejiang Leading Team of Science and Technology Innovation, the Postdoctoral Science Foundation of China (No. 2013M541774), the Preferred Postdoctoral Research Project Funded by Zhejiang Province (No. BSH1301016), and Swedish VR grant (# 621-2011-4620).

REFERENCES

1. McCreery, R. L., *Raman Spectroscopy for Chemical Analysis*, Wiley, New York, 2005.
2. Movasaghi, Z., S. Rehman, and I. U. Rehman, "Raman spectroscopy of biological tissues," *Applied Spectroscopy Reviews*, Vol. 42, No. 5, 493–541, 2007.
3. Lakowicz, J. R., "Radiative decay engineering: Biophysical and biomedical applications," *Analytical Biochemistry*, Vol. 298, No. 1, 1–24, 2001.
4. Novotny, L. and B. Hecht, *Principles of Nano-optics*, Cambridge University Press, 2012.
5. Otto, A., "The 'chemical' (electronic) contribution to surface-enhanced Raman scattering," *Journal of Raman Spectroscopy*, Vol. 36, 497–509, 2005.
6. Gabudean, A. M., M. Focsan, and S. Astilean, "Gold nanorods performing as dual-modal nanoprobes via metal-enhanced fluorescence (MEF) and surface-enhanced Raman scattering (SERS)," *The Journal of Physical Chemistry C*, Vol. 116, No. 22, 12240–12249, 2012.
7. Maier, S. A., *Plasmonics: Fundamentals and Applications*, Springer, New York, 2007.
8. Biagioni, P., J. S. Huang, and B. Hecht, "Nanoantennas for visible and infrared radiation," *Reports on Progress in Physics*, Vol. 75, No. 2, 024402, 2012.
9. Anger, P., P. Bharadwaj, and L. Novotny, "Enhancement and quenching of single-molecule fluorescence," *Physical Review Letters*, Vol. 96, No. 11, 113002, 2006.
10. Giannini, V., A. I. Fernández-Domínguez, S. C. Heck, and S. A. Maier, "Plasmonic nanoantennas: Fundamentals and their use in controlling the radiative properties of nanoemitters," *Chemical Reviews*, Vol. 111, No. 6, 3888–3912, 2011.
11. Kinkhabwala, A., Z. Yu, S. Fan, Y. Avlasevich, K. Müllen, and W. E. Moerner, "Large single-molecule fluorescence enhancements produced by a bowtie nanoantenna," *Nature Photonics*, Vol. 3, No. 11, 654–657, 2009.
12. Fromm, D. P., A. Sundaramurthy, P. J. Schuck, G. Kino, and W. E. Moerner, "Gap-dependent optical coupling of single "bowtie" nanoantennas resonant in the visible," *Nano Letters*, Vol. 4, No. 5, 957–961, 2004.
13. Mohammadi, A., V. Sandoghdar, and M. Agio, "Gold nanorods and nanospheroids for enhancing spontaneous emission," *New Journal of Physics*, Vol. 10, No. 10, 105015, 2008.
14. Aizpurua, J., P. Hanarp, D. S. Sutherland, M. Käll, G. W. Bryant, and F. G. De Abajo, "Optical properties of gold nanorings," *Physical Review Letters*, Vol. 90, No. 5, 057401, 2003.
15. Rakovich, A., P. Albella, and S. A. Maier, "Plasmonic control of radiative properties of semiconductor quantum dots coupled to plasmonic ring cavities," *ACS Nano*, Vol. 9, No. 3, 2648–2658, 2015.
16. Urban, A. S., X. Shen, Y. Wang, N. Large, H. Wang, M. W. Knight, and N. J. Halas, "Three-dimensional plasmonic nanoclusters," *Nano Letters*, Vol. 13, No. 9, 4399–4403, 2013.
17. Volpe, G., G. Volpe, and R. Quidant, "Fractal plasmonics: Subdiffraction focusing and broadband spectral response by a Sierpinski nanocarpet," *Optics Express*, Vol. 19, No. 4, 3612–3618, 2011.
18. Chen, T. L., D. J. Dikken, J. C. Prangsma, F. Segerink, and J. L. Herek, "Characterization of Sierpinski carpet optical antenna at visible and near-infrared wavelengths," *New Journal of Physics*, Vol. 16, No. 9, 093024, 2014.
19. Tok, R. U. and K. Şendur, "Plasmonic spiderweb nanoantenna surface for broadband hotspot generation," *Optics Letters*, Vol. 39, No. 24, 6977–6980, 2014.
20. Ünlü, E. S., R. U. Tok, and K. Şendur, "Broadband plasmonic nanoantenna with an adjustable spectral response," *Optics Express*, Vol. 19, No. 2, 1000–1006, 2011.
21. Boriskina, S. V. and L. Dal Negro, "Multiple-wavelength plasmonic nanoantennas," *Optics Letters*, Vol. 35, No. 4, 538–540, 2010.
22. Blanchard, R., S. V. Boriskina, P. Genevet, M. A. Kats, and F. Capasso, "Multi-wavelength mid-infrared plasmonic antennas with single nanoscale focal point," *Optics Express*, Vol. 19, No. 22, 22113–22124, 2011.

23. Pavlov, R. S., A. G. Curto, and N. F. van Hulst, "Log-periodic optical antennas with broadband directivity," *Optics Communications*, Vol. 285, No. 16, 3334–3340, 2012.
24. Navarro-Cia, M. and S. A. Maier, "Broad-band near-infrared plasmonic nanoantennas for higher harmonic generation," *ACS Nano*, Vol. 6, No. 4, 3537–3544, 2012.
25. Yang, J., F. Kong, K. Li, and S. Sheng, "Analysis of a log periodic nano-antenna for multi-resonant broadband field enhancement and the Purcell factor," *Optics Communications*, Vol. 342, 230–237, 2015.
26. Soliman, E. A., "Wideband nanocrescent plasmonic antenna with engineered spectral response," *Microwave and Optical Technology Letters*, Vol. 55, No. 3, 624–629, 2013.
27. Aouani, H., M. Rahmani, H. Sípová, V. Torres, K. Hegnerová, M. Beruete, and S. A. Maier, "Plasmonic nanoantennas for multispectral surface-enhanced spectroscopies," *The Journal of Physical Chemistry C*, Vol. 117, No. 36, 18620–18626, 2013.
28. Smolyaninov, A., L. Pang, L. Freeman, M. Abashin, and Y. Fainman, "Broadband metacoaxial nanoantenna for metasurface and sensing applications," *Optics Express*, Vol. 22, No. 19, 22786–22793, 2014.
29. Baffou, G., R. Quidant, and F. J. García de Abajo, "Nanoscale control of optical heating in complex plasmonic systems," *ACS Nano*, Vol. 4, No. 2, 709–716, 2010.
30. http://www.lumerical.com.
31. Johnson, P. B. and R. W. Christy, "Optical constants of the noble metals," *Physical Review B*, Vol. 6, No. 12, 4370, 1972.
32. Govorov, A. O. and H. H. Richardson, "Generating heat with metal nanoparticles," *Nano Today*, Vol. 2, No. 1, 30–38, 20077, 2007.
33. Purcell, E. M., "Spontaneous transition probabilities in radio-frequency spectroscopy," *Phys. Rev.*, Vol. 69, 681, 1946.
34. Sun, G., J. B. Khurgin, and R. A. Soref, "Practical enhancement of photoluminescence by metal nanoparticles," *Appl. Phys. Lett.*, Vol. 94, No. 10, 101103, 2009.
35. Rogobete, L., F. Kaminski, M. Agio, and V. Sandoghdar, "Design of plasmonic nanoantennae for enhancing spontaneous emission," *Optics Letters*, Vol. 32, No. 12, 1623–1625, 2007.
36. Chu, Y., M. G. Banaee, and K. B. Crozier, "Double-resonance plasmon substrates for surface-enhanced Raman scattering with enhancement at excitation and stokes frequencies," *ACS Nano*, Vol. 4, No. 5, 2804–2810, 2010.
37. Lin, J., Y. Zhang, J. Qian, and S. He, "A nano-plasmonic chip for simultaneous sensing with dual-resonance surface-enhanced Raman scattering and localized surface plasmon resonance," *Laser Photon. Rev.*, Vol. 8, No. 4, 610–616, 2014.
38. Palomba, S., M. Danckwerts, and L. Novotny, "Nonlinear plasmonics with gold nanoparticle antennas," *Journal of Optics A: Pure and Applied Optics*, Vol. 11, No. 11, 114030, 2009.
39. Noginov, M. A., G. Zhu, A. M. Belgrave, R. Bakker, V. M. Shalaev, E. E. Narimanov, and U. Wiesner, "Demonstration of a spaser-based nanolaser," *Nature*, Vol. 460, 1110–1112, 2009.